







# A survey on metasurface-based antennas for CubeSat spacecrafts

Boutaina Benhmimou<sup>1</sup> , Fouad Omari<sup>1</sup> , Nancy Gupta<sup>2</sup> , Khalid El Khadiri<sup>3</sup> ,  
Rachid Ahl Laamara<sup>1</sup> , Mohamed El Bakkali<sup>1,3,\*</sup> 

<sup>1</sup>LPHE-MS, Faculty of Sciences, University Mohammed V, Rabat, Morocco.

<sup>2</sup>ECE Department, Lyallpur Khalsa College Technical Campus, Jalandhar, Punjab, India.

<sup>3</sup>Department of Physics, Faculty of Sciences El Jadida, University Chouaib Doukkali (CDU), El Jadida, Morocco.

\*Corresponding author: [mohamed.elbakkali1617@gmail.com](mailto:mohamed.elbakkali1617@gmail.com)

## Review

Received:  
22 March 2025  
Revised:  
14 April 2025  
Accepted:  
7 May 2025  
Published online:  
1 June 2025

© 2025 The Author(s). Published by  
the OICC Press under the terms of  
the [Creative Commons Attribution  
License](#), which permits use, distribu-  
tion and reproduction in any medium,  
provided the original work is prop-  
erly cited.

## Abstract:

The Present CubeSat project success rate may deter nonprofit organizations from beginning new projects, especially for first-time creators. However, since the electronic components of a CubeSat are intended to be very power-efficient and tightly placed, its size and electrical characteristics provide a more difficult limitation. The CubeSat antennas are key parts that will need to be carefully designed since they need to be tiny, light, and deployable for bigger antennas. This study provides an extensive overview of the key characteristics of metasurface-based antennas with an emphasis on their effectiveness in CubeSat communication systems. This research work initially introduces metasurface antennas and examines how well-suited they are geometrically for various frequency bands for CubeSat spacecraft. Furthermore, a detailed analysis of these metasurface antennas' radiating capabilities is conducted in accordance with the CubeSat configuration, links, and orbits. Additionally, over thirty X-band metasurface-based antennas are fully evaluated in terms of their suitability for CubeSats. The use of specifically designed metasurfaces has resulted in a notable increase in CubeSat antenna performance. This paper offers an emerging approach for researchers to advance the usage of metasurface-based antennas in CubeSat missions such as UM5-Ribat and UM5-EOSAT CubeSats of University Mohammed V in Rabat.

**Keywords:** Metasurface-based antennas; Antenna gain; UM5-Ribat CubeSat; UM5-EOSAT CubeSat

## 1. Introduction

Modern technology has enabled the production of CubeSats weighing as little as 1.33 kg and with a typical volume of  $10 \times 10 \times 10 \text{ cm}^3$  [1]. Their potential has prompted the scientific community to reconsider the use of digital signal processing technologies, very large-scale integrated circuits, microelectromechanical systems, and low-power programmable systems to reduce the size and power consumption of electronics suitable for CubeSats. The revolutionary concept underlying the CubeSat, which is the subject of this article, is that designers may decrease satellite volume to the size of a secondary payload on conventional launch vehicles [3]. This significantly cuts launch costs, allowing universities, small commercial firms, government agencies, and even amateurs' fair access to space. Although the standardization and downsizing made possible by CubeSat spacecraft have received a lot of attention, the Poly

Picosatellite Orbital Deployer (P-POD) launch interface is the real breakthrough of CubeSats. All CubeSat developers are guaranteed to adhere to the same physical specifications thanks to this uniform deployment mechanism. With associated cost and schedule benefits, the P-POD attempts to separate the spacecraft's development, integration, and verification from those of the launch vehicle as much as feasible. Over the previous two decades, the bulk of CubeSat projects have been employed for Low Earth Orbit (LEO) applications [4]. A number of obstacles stand in the way of CubeSats' deep space exploration efforts, including adequate DC power, the size limitation of each subsystem, and the lack of a large enough RF aperture for research payload and communication [5]. In contrast, a deep space mission must sustain a minimum 2 million km link back to Earth, whereas an LEO spacecraft may have a maximum communication range of only 2,000 kilometers [1]. In this scientific and technological momentum, the CubeSat,

which appeared at the beginning of the third millennium, is of utmost importance due to its extraordinary flexibility and the possibility of being installed in a period not exceeding a few weeks [1, 4]. When the CubeSat/dispenser package was initially conceptualized, the plan was to attach the dispenser to the rocket for many CubeSat flights where space was available [6]; see figure 1. This is the number of CubeSats that are still launched in groups and linked together to create dispersed satellite arrays of sensors in orbit. Keep in mind that any rocket, under the right conditions, may be a CubeSat launch vehicle. As a result, it may have a higher performance margin, be capable of reaching the appropriate orbit, and be modified to allow dispensers to be fitted [7]. This possibility of launching dozens in one flight or considering them as a secondary payload for missions transporting food and equipment to the International Space Station reduces the costs to such an extreme extent that it makes us believe that our true homeland and our bright future are in space and with this technology [2]. For example, SpaceX realizes an average of weekly launches over a year and the possibility of reusing their launch vehicles, which goes beyond the traditional terminology such as failure or faltering [8].

Since it is the sole way for the consumer to communicate with the satellite while it is in orbit using the proper antennas, the communications system of the satellite is still generally regarded as the most crucial component. Without it, the spacecraft is little more than space debris. In addition to easing data flow from satellite orbit to the ground, it also performs tracking, telemetry, and command functions. The communication subsystems consist of an Earth-based base station, CubeSat antennas, and transceivers [1]. It might have a custom-built transmitter or a modified or unmodified COTS radio. These transceivers must be capable of error detection and correction, as well as transmitting and receiving encapsulated and decapsulated serial data. Moreover, when we consider that the satellite rotates around the Earth many times a day, the whole mission of the spacecraft is contingent upon the properties of the chosen antenna. Additionally, in order to comply with the CubeSat standard's weight and size constraints, designers are forced to reduce connection quality due to the intrinsic proportionality between antenna gain and antenna size [9]. Adhering to these specifications while preserving optimal performance poses a significant radiofrequency and mechanical difficulty. With CubeSats being assessed for advanced low-Earth orbit and deep-space missions, the scientific community is actively developing innovative antenna systems that can match data

rate and resolution standards while minimizing the antenna system's physical size.

In this regard, antenna systems are of utmost importance for remote sensing and thus connecting the user on the ground with the CubeSat, even if only for a few minutes a day, due to the advantages of the antennas used. We point out that CubeSat communication systems consume about 2 watts in total, and therefore relying on amplifiers to improve the performance of the used antennas may leave the rest of the devices without power and thus fail the entire mission [1, 4]. The limitations of batteries and solar panels on board each CubeSat unit make it a difficult challenge to distribute power equitably to all devices, which requires constant monitoring. Therefore, planning long-range missions or increasing the data exchanged per day, which sometimes takes place in only a few minutes, is far from any protection in the case of adopting amplifiers and is not a primary solution. This challenge opened the door wide for antenna engineering specialists to work creatively in developing unconventional antenna systems usable in missions, including both outer space and low-Earth orbit [1, 9]. With potential CubeSat missions operating over a broad range of frequencies, from ultrahigh frequencies (UHF) (400 MHz) up to 110 GHz (W band), a variety of antenna configurations for CubeSat spacecraft have been suggested in the literature. Owing to their low profile and relative ease of fabrication, planar antennas, such as patch and slot antennas, have gained special attention for CubeSats [10, 11]. An example of patch antennas seamlessly integrating into the CubeSat chassis for a specific CubeSat mission is illustrated in figure 2.

This study aims to thoroughly examine the properties of numerous existing metasurface-based antennas that have been provided to the scientific research community in order to answer concerns about how well they may be modified and developed to be successful on CubeSats. This paper was presented within a strategic framework in which the characteristics of analyzed metasurface-based antenna designs are in harmony with the properties of the CubeSat for the mission's overall success with little expense and minimal electricity use. The paper is organized in the following manner. Section 1 surrounds the works that this study targeted by examining and summarizing their essential geometrical and mechanical characteristics in relation to a specific CubeSat mission. Section 3 summarizes the performance of all analyzed metasurface-based antenna systems discussed in section 2 and evaluates their suitability for use on CubeSats. Section 4 evaluates tens of AMC and metasurface-based antenna systems for X-band CubeSat communication. Finally,

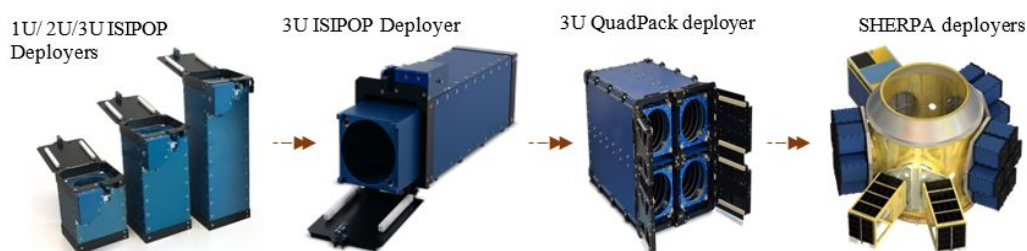
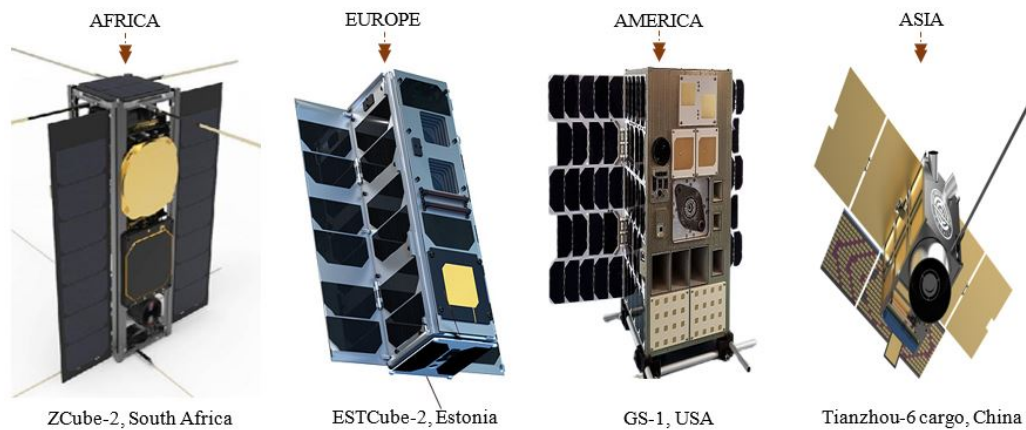


Figure 1. Standard and smart CubeSat deployers [2].



**Figure 2.** CubeSat spacecrafts with planar antennas from continents of Africa, Europe, America, and Asia [8].

section 5 wraps up the work with a review of major findings and recommendations for further research.

## 2. Quantitative analysis: Mechanisms and alternative approach for CubeSats and ultra-small spacecrafts

The first study on the characteristics of materials with simultaneous negative permittivity and permeability was published by Veselago in 1968 [22]. These materials are referred to as LHMs because, like electromagnetic waves, their group and phase velocities are reversed and propagate in the opposite direction [42]. The literature [22] provides extensive documentation on the evolution and history of metamaterials. Because of their significant loss, materials having a negative refractive index are exceedingly challenging to develop and employ in practical applications. They also feature restricted bandwidth, high dispersion, and anisotropic properties. In this regard, researchers are looking at metamaterials with various extreme values, such as ZIM, ENZ, MNZ, and PMC materials, in addition to DNG materials. Permittivity and permeability may be applied to these materials with a positive value, enabling production and practical applications. Specifically, Sievenpiper et al. (1999) used a PMC with the HIS of a periodic mushroom structure made up of patches and vias. Since then, other structures with features similar to this, HIS structure have been discovered, including reactive impedance surfaces and EBG structures, which are collectively referred to as AMC. Thus, many metamaterials may be characterized as materials in new or artificial structures that have been developed to exhibit qualities that are either absent or difficult to achieve in nature. Unlike PEC, AMCs exhibit no phase shift when an electromagnetic wave is incident and reflected vertically. The current flowing in the conductor of the AMC is in the same direction as the imaging current created in it. Such a physical phenomenon, known as constructive interference, can enhance antenna properties even when the antenna is placed very close to the AMC, which can be highly advantageous for antenna downsizing and development. A metasurface structure, which implements AMC features through a periodic surface made up of a single layer, has lately gained interest. The metasurface structure is realized

in two dimensions and thus requires a small physical space; this is in contrast to general metamaterials, which have a three-dimensional structure. These properties open the door to the development of new theory and applications as detailed in [43, 44], and many excellent review articles on the fundamentals and applications of metasurfaces can be found in references [45–48]; see figure 3.

All of the metamaterials used in this work are referred to as metasurface-based throughout this paper. A metasurface, which is a two-dimensional equivalent of a metamaterial, is essentially a surface distribution of electrically small scatterers that can manipulate and control electromagnetic waves. The functionality of the metasurfaces is governed by the specific geometrical shape of the scatterers that are fabricated on the dielectric substrate. Metasurfaces can provide the novel characteristics of an ultra-low profile and enhanced performance in gain, radiation pattern, and bandwidth. These metasurfaces have many other inherent advantages, such as low cost, low mass, extreme flatness, and easy fabrication, which have led to metasurface research expanding from microwave to optical frequencies, and many extraordinary properties of metasurface antennas have been demonstrated. In this paper, an attempt is made to review tens of metasurface-based antenna designs and study their suitability for CubeSats. One major concern regarding antennas that use a metasurface is the existence, due to the presence of a finite-size metasurface structure, of resonances that are additional to the conventional resonance created in the main radiating element. Table 1 provides the design characteristics of many metasurface-based antennas, including physical dimensions, construction materials, frequency ranges, and the suitable configuration. This comprehensive data enables a quick comparison of all of the described metasurface-based antenna designs, as well as revealing their mechanical and geometrical qualities, allowing researchers to investigate their potential for usage on CubeSats. Furthermore, the thorough information supplied in Table 1 allows engineers to make educated judgments when choosing a metasurface antenna design that best meets their CubeSat mission objectives. Additionally, by studying these design factors, researchers may improve the performance of these antennas for diverse communication needs in CubeSat missions.



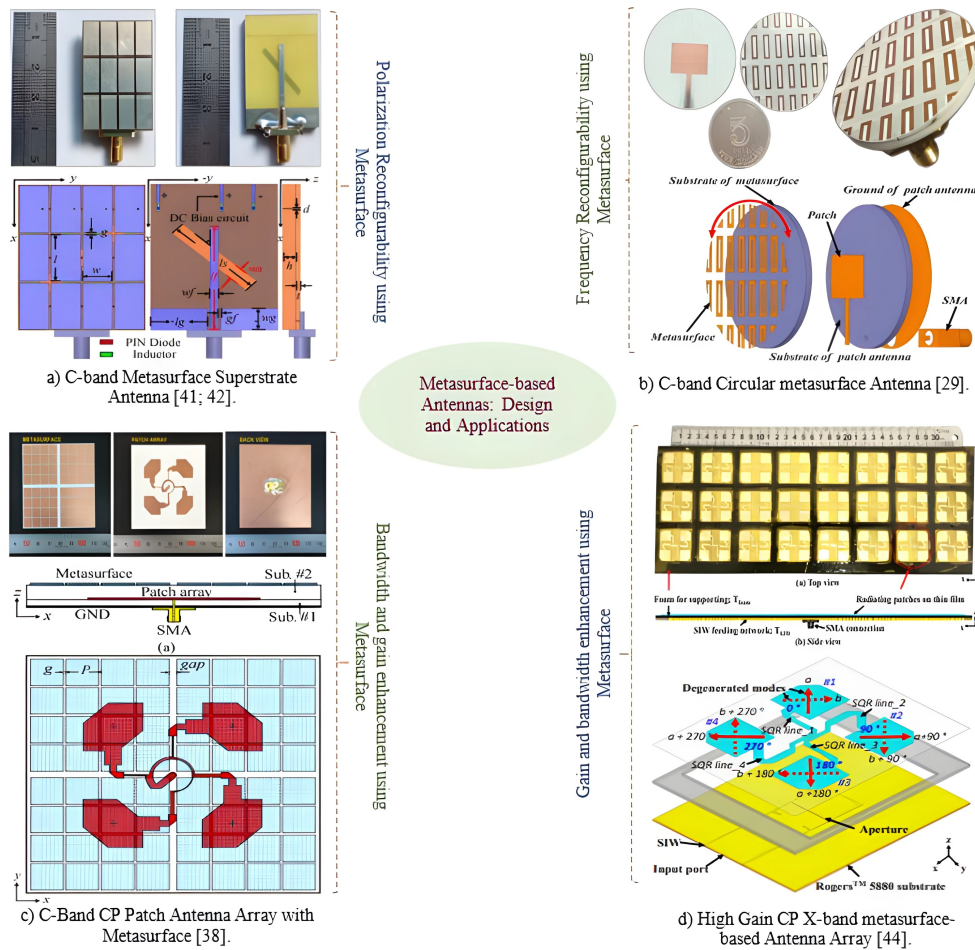


Figure 3. Various design and roles of metasurface-based antennas.

Table 1. Geometrical comparison between some metasurface-based antennas proposed by the scientific community.

Ref.	Antenna size (mm <sup>3</sup> )	Materials	Oper. fr. [GHz]	CubeSat
L-Band				
[12]	120×120×16.3	Rogers RO4003 ( $\epsilon_r=3.38$ , $\tan \delta=0.0027$ , $h_1=h_2=0.8128$ mm)	1.76	6U, 8U, 12U
[13]	80×80×8.76	Rogers RT4003 ( $\epsilon_r=3.55$ , 1.62 mm-thick)	1.09	1U, 1.5U, 2U
S-Band				
[14]	120×120×23.1	FR4 and Rogers 3003	2.40	6U, 8U, 12U
[15]	45×40×1.524	Rogers-4003 ( $\epsilon_r=3.55$ , $\tan \delta=0.0027$ , 1.524 mm-thick)	3.60	0.5U, 1U, 1.5U
[16]	70×70×3	Rogers RO4003 ( $\epsilon_r=3.38$ , $\tan \delta=0.0027$ )	3.50	1U, 2U, 3U
[17]	129×101×3.2	FR4, copper	2.10	1.5U, 2U, 3U, 6U
[18]	96.5×96.5×2.242	RO4350 ( $\epsilon_r=3.66$ , $\tan \delta=0.004$ , 0.762 mm and 1.542 mm-thicks)	MS: 2.49 NMS: 2.45	1.5U, 2U, 3U
[19]	25.2×23.7×10	RT/duroid 5880 (0.5 mm-thick)	2.40; 3.50	0.5U, 1U, 1.5U
[20]	50×50×1.6	FR4; Copper	2.45 3.5	0.5U, 1U, 1.5U, 2U
[21]	443×350×9	F4B materials	2.80-3.76	12U, 16U, 27U

Continued of Table 1.

Ref.	Antenna size (mm <sup>3</sup> )	Materials	Oper. fr. [GHz]	CubeSat
<b>C-Band</b>				
[23]	64×64×2.34	Rogers RO4003 ( $\epsilon_r=3.38$ and $\tan \delta=0.0027$ ; $h_1=0.8128$ mm and $h_2=1.524$ mm)	5.50	0.5U, 1U, 1.5U
[24]	78×60×1.6	FR4 ( $\epsilon_r=4.2$ , $\tan \delta=0.022$ , 1.6 mm-thick) FR4 ( $\epsilon_r=4.2$ , and $\tan \delta=0.022$ , 3.2 mm-thick)	4.20	1U, 1.5U, 2U
[25]	40×40×1.524	RO4350B ( $\epsilon_r=3.48$ , 1.524 mm-thick)	5.60	0.5U, 1U, 1.5U
[26]	39.2×40×4.76	dielectric substrate ( $\epsilon_r=3.6$ and $\tan \delta=0.003$ ), copper	5.60	0.5U, 1U, 1.5U
[27]	64×64×4.8	Arlon AD450 ( $\epsilon_r=4.5$ and $\tan \delta=0.0035$ ), copper	5.42	1U, 1.5U, 2U
[28]	35×35×0.762	RO4350B ( $\epsilon_r=3.5$ , $\tan \delta=0.004$ , 0.762 mm-thick)	4.00	0.5U, 1U, 1.5U
[29]	33.5×22.5×3	FR4 ( $\epsilon_r=4.4$ , $\tan \delta=0.01$ , 3 mm-thick)	4.90	0.5U, 1U, 1.5U
[30]	40.8×30.4×4	F4B ( $\epsilon_r=2.65$ , $\tan \delta=0.002$ )	5.50	0.5U, 1U, 1.5U
[31]	54×54×3.81	Rogers RO4350B ( $\epsilon_r=3.66$ , $\tan \delta=0.004$ )	7.50	1U, 1.5U, 2U
[32]	64× 64 × 2.34	Rogers RO4003 ( $\epsilon_r=3.38$ , $\tan \delta=0.0027$ , 0.812 and 1.524 mm-thicks), copper (17 $\mu$ m-thick)	6.00	1U, 1.5U, 2U
[33]	60.0×88.0× 4.8	FR4 ( $\epsilon_r=4.3$ , $\tan \delta=0.02$ , 3.2 mm and 1.6 mm-thicks)	4.00	1U, 1.5U, 2U
[34]	40×40×1.524	Rogers substrates RO4350B (1.524 mm-thick)	4.77, 5.07, 5.51	0.5U, 1U, 1.5U
[19]	25.2×23.7×10	RT/duroid 5880 (0.5 mm-thick)	5.50	0.5U, 1U, 1.5U
[20]	50×50×1.6	FR4; Copper	5.75 7.50	0.5U, 1U, 1.5U, 2U
<b>X-Band</b>				
[35]	8.5×11.4×11	Copper	9.50	0.5U, 1U, 1.5U, 2U
<b>Ku-Band</b>				
[36]	340×137×1.408	Copper (0.1 mm-thick), Polyimide film ( $\epsilon_r=3$ , 0.8 mm-thick)	12.00	12U, 16U, 27U
[15]	45×40×1.524	Rogers-4003 ( $\epsilon_r=3.55$ , $\tan \delta=0.0027$ , 1.524 mm-thick)	14.33	0.5U, 1U, 1.5U, 2U
<b>Ka-Band</b>				
[37]	5.2×5.2×2.33	F4B ( $\epsilon_r=2.2$ , $\tan \delta=0.001$ , 1.5 mm-thick), Copper (18 $\mu$ m-thick)	26.00	0.25U, 0.5U, 1U, 1.5U
[38]	13.5×13.5×0.162	Rogers RT5880 ( $\epsilon_r=2.2$ , 0.127 mm-thick), Copper (0.035 mm-thick)	24.0; 27.0; 29.0; 36.0; 38; 40.5; 41.0	0.25U, 0.5U, 1U, 1.5U
[15]	45×40×1.524	Rogers-4003 ( $\epsilon_r=3.55$ , $\tan \delta=0.0027$ , 1.524 mm-thick)	28.89	0.5U, 1U, 1.5U, 2U
<b>W-Band</b>				
[39]	44.5×49×0.525	Silicon (Si) ( $\epsilon_r=11.9$ ), Gallium Arsenide (GaAs) ( $\epsilon_r=12.8$ )	94.00	0.5U, 1U, 1.5U, 2U
<b>THz-Band</b>				
[40]	1.905×1.905×0.08	GaAs ( $\epsilon_r=12.9$ , $\tan \delta=0.006$ , 40 $\mu$ m-thick (0.375THz), 80 $\mu$ m-thick (0.33 THz))	385 375 330	0.1U, 0.25U, 0.5U, 1U
[41]	1.8×1.8×0.04	GaAs ( $\epsilon_r=12.9$ )	342	0.1U, 0.25U, 0.5U, 1U

According to the antenna characteristics for a particular CubeSat design, the research findings listed in Table 1 above, which target various frequency bands, provide appropriateness for CubeSat configurations ranging from Zep-toSats and FemtoSats to 6U, 8U, 12U, and 27U. All of them are provided in terms of physical dimensions, materials, operating frequency, and the appropriate CubeSat design for the desired frequency range. For example, the metasurface-based antenna designs provided in references [15, 19, 20] that target S-band; [19, 20, 23, 25, 26, 28–30, 34] that target C-band; [15] that target Ku and Ka-bands; and [39] that target W-band are geometrically and mechanically suitable for all CubeSat configurations, including 0.5U, 1U, 1.5U, and 2U. They are low-profile, small in size, have minimal power consumption, and do not require any deployment equipment. Furthermore, the contributions introduced in references [35] for X-band, [37, 38] for Ka-band, and [40, 41] for THz-band are the smallest designs, occupy very little volume, and have mass less than 10 g, making them all very good candidates for ultra-small spacecraft such as ZeptoSats, FemtoSats, and 0.25U CubeSats. In addition to that, the antenna approaches described in [13] for the L-band, [16, 18] for the S-band, and [24, 27, 31–33] for the C-band have geometries and mechanical characteristics that make them ideal for use on 1U, and therefore, 2U and 3U CubeSats. They don't require any

deployment systems and are lightweight. The metasurface-based antenna designs found in references [12, 14, 21] are geometrically suited for 6U configurations with volumes of  $30 \times 20 \times 10 \text{ cm}^3$ , which are launched in advanced LEO and interplanetary missions. Since it does not require a deployment system and consumes little electrical power, the design presented in [21] can be, geometrically and mechanically, used in 12U, 16U, and 27U configurations. The next section will offer a full review of the capabilities of all the studies indicated in Table 1 to illustrate their effectiveness for a specific CubeSat design as a whole.

### 3. Qualitative analysis

As previously said, the performance of the selected antenna is critical to the CubeSat mission as a whole, especially when considering the speed of the satellite's movement around the Earth numerous times each day. Table 2 summarizes the radiating performance of all research works examined and evaluated in the preceding section, demonstrating that diverse metasurface-based antenna designs may operate throughout all frequency bands. Note that the geometrical, mechanical, and electrical properties of suggested antennas are examined to determine their appropriateness for a CubeSat project. As a result, if an antenna system meets all of the mission's geometrical, mechanical, and

**Table 2.** Radiating performances on various metasurface-based antenna designs.

Ref.	Oper. fr. [GHz]	Gain [dBi]	Ant. pol.	BWs [GHz]	rad. pattern	EMI
<b>L-Band</b>						
[13]	1.09	6.98	L.P.	-10 dB BW: 0.017	U.D.	very low
[12]	1.76	8.20	L.P.	-10 dB BW: 1.39-2.09	U.D.	very low
<b>S-Band</b>						
[14]	2.40	SA: 5.86 MSA: 5.84	RHCP LHCP	3 dB ARBW: 2.47-2.55 -10 dB BW: 2.41-2.59	B.D.	high
[17]	2.10	7.50	L.P.	-10 dB BW: 0.0351	U.D.	very low
[16]	3.50	8.60	L.P.	-10 dB BW: 3.14-3.83	U.D.	low
[18]	MS: 2.49 NMS: 2.45	MS: 5.69 NMS: 6.43	C.P.	-10 dB BW: 0.051 3 dB ARBW: 0.113	U.D.	low
[15]	3.6	6.47	L.P.	-10 dB BW: 2.76-6.47	B.D.	high
[19]	2.40; 3.5	0.4; 0.70	L.P.	-10 dB BW: $\sim 0.30$	B.D.	high
[20]	2.45 3.5	2.04, 0.634	L.P.	-10 dB BW: $\sim 2.4$ -2.5 -10 dB BW: $\sim 3.5$ -3.70	B.D.	high
[21]	2.80-3.76	22.20	L.P.	-10 dB BW: 2.81-3.76	U.D.	low
<b>C-Band</b>						
[23]	5.50	11.60	C.P.	-10 dB BW: 4.56-6.98 3 dB ARBW: 4.67-6.39	U.D.	low
[24]	4.20	7.40	C.P.	3 dB ARBW: 3.7-4.5	U.D.	low
[25]	5.60	7.70	C.P.	-10 dB BW: 5.48-5.70	U.D.	low
[26]	5.60	$\sim 8.0$	C.P.	-10 dB BW: 4.7-6.5 3 dB ARBW: $\sim 5.4$ -6.5	U.D.	low

Continued of Table 2.

Ref.	Oper. fr. [GHz]	Gain [dBi]	Ant. pol.	BWs [GHz]	rad. pattern	EMI
[27]	5.42	9.30	C.P.	3 dB ARBW: 5.37-6.25	U.D.	low
[29]	4.90	5.8	C.P.	-10 dB BW: 4.2-5.90 3 dB ARBW: 4.9-5.90	U.D.	medium
[30]	5.50	PIN OFF: 7.0 PIN ON: 6.1	C.P. L.P.	-10 dB BW: 5.1-6.4 3 dB ARBW: 5.4-6.4	U.D.	medium
[31]	7.50	9.18	L.P.	-10 dB BW: 4.81-9.69	B.D.	high
[32]	5.90; 6.0	12.08	C.P.	-10 dB BW: 4.40-8.00 3 dB ARBW: 4.75-7.25 3 dBi GBW: 4.8-7.0	U.D.	low
[33]	4.0	7.0-7.50	C.P.	3 dB ARBW: 3.62-4.75	U.D.	very low
[34]	4.77 5.07 5.51	5.30 5.50 5.40	L.P.	-10 dB BW: 4.76-5.51 (0.75)	U.D.	low
[28]	4.0	Patch 1: 4.95 Patch 2: 4.35	L.P.	-10 dB BW: 3.96-4.05	U.D.	low
[19]	5.50	2.64	L.P.	-10 dB BW: ~ 3.0-7.0	B.D.	high
[20]	5.75 7.50	5.6 4.69	L.P.	-10 dB BW: ~ 5.5-60 -10 dB BW: ~ 7.50-8.0	B.D.	high
<b>X-Band</b>						
[35]	9.50	16.90	L.P.	-10 dB BW: ~ 9.5-10.5	U.D.	low
<b>Ku-Band</b>						
[15]	14.33	6.71	L.P.	-10 dB BW: ~ 13.0-15.0	M.L.	medium
[36]	12.00	26.40	C.P.	3 dB ARBW: 11.55-12.25	U.D.	very low
<b>Ka-Band</b>						
[38]	27; 29.0; 36; 38; 40.5; 41.0	10; 9.98; 10.7; 12.6; 9.46; 9.30	L.P.	-10 dB BW: 23.75-28.8 -10 dB BW: 36.22-40.5	M.L.	medium
[15]	28.89	7.73	L.P.	-10 dB BW: 27.0-31.0	M.L.	medium
[37]	26.00	30.70	L.P.	3 dBi GBW: 24.1-28.2 -10 dB BW: ~ 25.0-29.0	U.D.	very low
<b>W-Band</b>						
[39]	94.00	~ 18.0	L.P.	Not assigned	U.D.	low
<b>THz-Band</b>						
[40]	385 375 330	5×3cells: 12.5 5×6cells: 15.5 5×12cells: 18.5	L.P.	3 dBi GBW: ~ 50 (0.08 mm), ~ 65 (0.04 mm), ~ 40 (0.02 mm)	U.D.	low
[41]	342	15.50	L.P.	3 dBi GBW: 342-408	U.D.	very low

electrical requirements, it may be utilized for the CubeSat mission targeting direct-to-Earth station, CubeSat swarm, or CubeSat constellation applications. According to figure 4, a spacecraft like a CubeSat can communicate with earth stations directly, through a mothership, or through a CubeSat constellation. This depends on the CubeSat's transmitting power ( $P_t$ ) and transmitting gain ( $G_t$ ), the mothership's or earth station's receiving power ( $P_r$ ) and receiving gain ( $G_r$ ),

and the free space wavelength ( $\lambda$ ), which is determined by the targeted frequency band.

The metasurface-based antenna designs described in references [18, 23–27, 29, 30, 32, 33, 36] radiate unidirectionally and attain –10 dBi bandwidths around various operating frequencies targeting distinct frequency bands. They are also circularly polarized and attain high 3 dB axial ratio bandwidths with gains ranging from 5.69 dBi at an





all geometrical and mechanical requirements for ultra-small spacecrafts like ZeptoSats and FemtoSats. Their radiation patterns are unidirectional, with peak gains of 12.5 dBi at 385 GHz (THz-band) [41],  $\sim 18.0$  dBi at 94 GHz (W-band) [39], 18.5 dBi at 330 GHz (THz-band) [40], and 30.70 dBi at 26.0 GHz (Ka-band) [37]. The multi-band metasurface-based antenna designs shown in references [15, 38] operate at Ku and Ka-band along ultra-wide impedance bandwidths of 23.75 – 28.8 GHz and 36.2 – 24.5 GHz [38] and 13.0 – 15.0 and 27.0 – 31.0 GHz [15], with peak gains ranging from 6.71 dBi at 14.33 GHz [27] to 12.6 dBi at 38 GHz [38]. These performances and physical sizes are ideal for all CubeSat structures, including 0.25U and 0.5U for inter-CubeSat communications or direct-to-earth if a large ground station is used to ensure communication links between consumers on Earth and the spacecraft in orbit as it moves around the planet. Furthermore, their multilobe radiation patterns demonstrate how to use multiple floors of metasurface arrays to combine the obtained effective bands and radiating lobes into a single lobe and frequency band, respectively. This results in unidirectional, wideband, and high-gain antenna systems, which increases their suitability for advanced LEO and interplanetary CubeSat missions as well as CubeSat constellations as “motherships.”

Antenna configurations proposed in [14, 19, 20, 31] satisfy all geometrical and mechanical criteria of all CubeSat forms

while radiating bidirectionally, and thus their major weakness that limits their effectiveness for space applications is the very high interference with other circuits inside the satellite box. From another perspective, they provide poor gains and so cannot be employed for limitless lifespan CubeSat missions. To address these issues, a cavity reflector or an array of AMC unit cells can be placed beneath these antenna designs to forward back lobe radiations and therefore improve their performance by eliminating produced interferences that restrict the success rate of a CubeSat mission. These guidelines are utilized to conduct a detailed examination of a certain frequency band, which is the X-band in the next section.

#### 4. X-band AMC, metamaterial and metasurfaced antennas for CubeSats

In this section, the X-band is extensively studied because of its potential to design high-performing medium- and small-sized planar antennas. The goal is to balance the trade-off between improving the antenna performances for direct-to-Earth communications and maintaining geometrical suitability for all CubeSat configurations, including 0.5U and 1U structures. This results in a metasurface unit cell that is smaller than 1 cm by 1 cm in a compact area, making the whole metasurface-based antenna adaptable to any CubeSat layout. Tables 3, 4, and 5 demonstrate that over 25 X-band

**Table 3.** Comparison between various AMC-based antenna designs for CubeSats at X-band.

Ref.	Antenna size (mm <sup>3</sup> )	Oper. fr. [GHz]	Gain [dBi]	BWs [GHz]	Rad. pattern	EMI
[49]	PSA-AMC: 75×78×4	6.63-13.73	11.10	-10 dB BW: 1.5	U.D.	low
	Bowtie-AMC: 50×70×25	6.98-8.57	13.0	-10 dB BW: 6.1		
[50]	28.5×29×1.34	7.85-12.24	12.3	-10 dB BW: 4.4 7-13.32	U.D.	minimum
[51]	112×58×3.5	7.43-11.7	11.95	7.43-11.7	B.D.	high
[52]	50×26×0.5	2.75	7.19	2.6-2.8	Semi-O.D.	medium
		5.50	5.95	5.3-5.6		
		7.60	6.17	6.9-8.8		

**Table 4.** Comparison between various metamaterial antenna designs for CubeSats at X-band.

Ref.	Antenna size (mm <sup>3</sup> )	Oper. fr. [GHz]	Gain [dBi]	BWs [GHz]	Rad. pattern	EMI
[53]	56.4×56.4	8.725	11.813	-10 dB BW: 0.157	B.D.	high
		8.812	10.216	0.073		
		9.189	10.860	0.067		
		9.999	9.9385	0.042		
		10.362	11.164	0.132		
		11.147	13.130	0.104		
		10.920		0.114		
[54]	15×25	13.22	6.02	-10 dB BW: 5.75	B.D.	minimum
[55]	40×30×0.8	9.70	8.43	-10 dB BW: 1.60	U.D.	low
[56]	96×96	3.1-3.5	7.6	3.1-3.5	U.D.	low
	96×270	8.6-9.6	13.7	8.6-9.6		
[19]	25.2×23.7×10	8.30	1.70	-10 dB BW: $\sim 8.0$ -10.0	B.D.	minimum
[57]	70×60	9.40	17.10	-10 dB BW: 0.2	U.D.	very low
[58]	55×55×17.67	10.00	9.45	-10 dB BW: 9.42-10.62	U.D.	reduced
[59]	30×22×1.6	10.10	7.20	-10 dB BW: 8.50-11.30	U.D.	low

**Table 5.** Comparison between various metasurface antenna designs for CubeSats at X-band.

Ref.	Antenna size (mm <sup>3</sup> )	Oper. fr. [GHz]	Gain [dBi]	BWs [GHz]	rad. pattern	EMI
[60]	12×12×3.58	8.95-10.68	5.85	-10 dB BW: 8.95-10.68 3 dB ARBW: 10.62-11.87	U.D.	minimum
[61]	140×140	8.82, 9, 9.25, 9.43, 10.1	not assigned	-10 dB BW: 8.5-10.5	U.D.	negligible
[62]	28×28	10.44	7.57	-10 dB BW: 10.14-10.94	U.D.	medium
[63]	~74×74	LP: 9.5-10.2 CP: 10.2-10.8	10.00	-10 dB BW: 8.0-12.0	U.D.	low
[64]	~24×24×2.004	10.0	8.60	-10 dB BW: 8.41-11.67	U.D.	very low
[65]	50×50	7.80; 8.10	8.60	-10 dB BW: 7.25-8.40	B.D.	high
[66]	281.148×80×4.7	10.65	11.6-13.4	-10 dB BW: 0.20	U.D.	low
[67]	~20×20×2	10.0	15.60	-10 dB BW: ~7.0-13.5	U.D.	low
[68]	~31.2×31.2×4.5	7.47-11.65	H: 6.58-7.68 V: 5.85-7.28	H: 7.47-11.65 V: 7.66-11.33	Quasi-O.D.	low
[69]	140×135×4.8	11.30	9.25-19.7	-10 dB BW: 10%	U.D.	very low
[70]	62×62×22.2	8.28-8.88	7.0	-10 dB BW: 8.0-9.5 3 dB ARBW: ~8.3-8.8	U.D.	low
[71]	~180×180×3.5	10.40	18.20	~9.0-12.0	U.D.	very low
[72]	~81.75×81.75×14.3	10.90 22.50	8.40 6.40	3 dB ARBW: 10-12.54 21.82-24.57	U.D.	low
[73]	~25×25×12	8.53-8.91 8.56-8.89	~10.0	8.53-8.91 8.56-8.89	U.D.	low
[74]	60×60×7.92	3.12-5.92 7.14-8.45	7.6±1.50 7.4±1.80	3.1-6.20 7.1-8.70	U.D.	low
[75]	~34×40×6	10	16.50	9.75-11.0	U.D.	low
[76]	80×80	10.0-13.0	13.40	3 dB ARBW: 3.5 (9.5-13) -10 dB BW: 3.3 (9.5-12.8)	U.D.	low
[77]	390×390×2.3	9.0-10.60	27.70	-10 dB BW: 9.2-10.50	U.D.	low
[78]	112×112	10.0	17.90	-10 dB BW: 9.7-10.7	U.D.	low
[79]	29×29×2	8.40	5.80	-10 dB BW: 8.28-8.59	U.D.	low

AMC, metamaterials, and metasurface-based antennas have physical sizes that are adequate for 1U CubeSat, with the majority being extremely suitable for 0.5U constructions. They are lightweight, have minimal power consumption, and exhibit good radiating properties, making them ideal for X-band CubeSat communications. The stated X-band metasurface-based antenna designs are thoroughly examined in terms of physical dimensions, operating frequency, materials, polarization, forms of realized radiation patterns, and the amount of created interference. Most studied antennas are circularly polarized, radiate unidirectionally, and provide ultra-wide effective bands. For instance, an ultra-small volume of  $29 \times 29 \times 2 \text{ mm}^3$  is occupied by an X-band metasurface-based antenna, which achieves the lowest peak gain value of more than 5.80 dBi [79]. Additionally, the antenna system described in reference [57] is printed on an inexpensive Rogers 4003C dielectric for operation at 9.40 GHz, radiates unidirectionally, and achieves a high gain of 17.10 dBi, making it suitable to target advanced LEO CubeSat missions or, if the right Earth station is used, inter-

planetary links [80]. Its small area of  $70 \times 60 \text{ mm}^2$  makes it suitable for 1U CubeSat and hence all other configurations [81–88].

To show more effectiveness of metasurface-based antennas for X-band CubeSat communications, a  $50 \Omega$  probe-fed cross-patch antenna with metasurface mentioned in [79] that is mounted to Rogers RO 4003 dielectric material, which has a thickness of 2 mm, a loss tangent of  $\tan \delta \approx 0.002$ , and a relative permittivity of  $\epsilon_r = 3.55$ , in order to further demonstrate the efficacy of X-band metasurface antennas for CubeSat and ultra-small spacecrafts. As illustrated in figure 5, the design features a compact crossing antenna coupled with a metasurface comprising  $10 \times 10$  tiny unit cells. This metasurface is placed between the ground plane and the cross-patch antenna, situated 0.4 mm below the active radiating element [79]. The ANSYS HFSS software's Finite Element Method is used to design and compute the parameters of the created sandwiched metasurface antenna. The Quasi Newtonian Method (QNM), a package of the ANSYS HFSS, is used to optimize the metasurface's per-

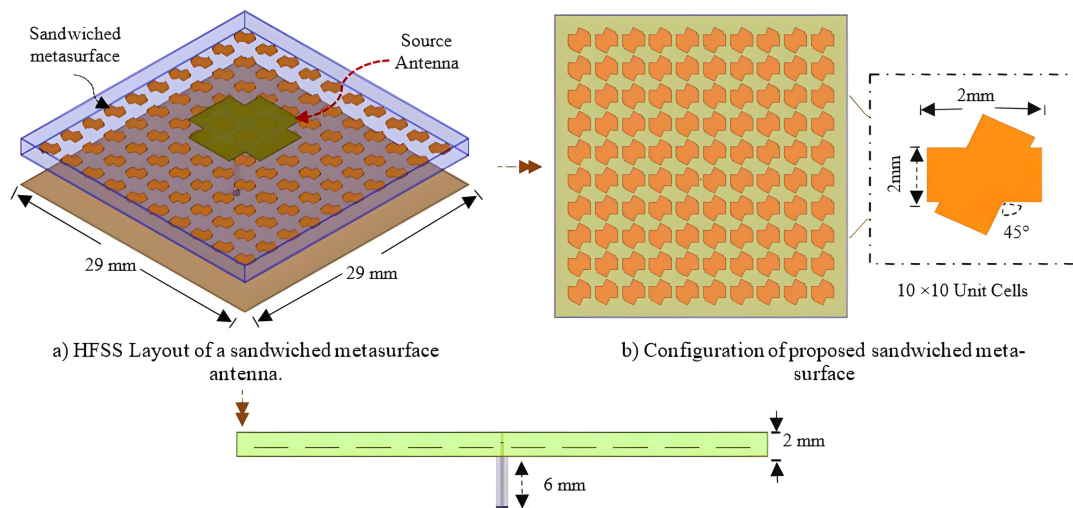


Figure 5. Geometry of an X-band sandwiched metasurface antenna [79].

formance and reduce its size. Using a  $50\ \Omega$  coaxial probe with a 6 mm length and 0.05 mm radius, the cross-patch antenna is excited and coupled to the first one on the geometric center of the antenna. The unit cells selected for the proposed metasurface design are square closed rings, which can be adapted with a limited number of parameters and optimized with an easy QNM program. The optimized unit cells are placed with a 1 mm inter-cell distance, measuring 4 mm in length and 2 mm in width. The suggested unit cell structure's two strips are inclined at a  $45^\circ$  angle to fit into a very small space on the bodies of ultra-small spacecraft such as FemtoSats and 0.5 CubeSats. Therefore, the focus of our suggested antenna technique is on the gain increase and return loss of a probe-excited crossing antenna at an X-band operating frequency of 8.4 GHz, which is suitable for extremely small and ultra-compact spacecrafts like FemtoSats. The goal of this contribution is to design an extremely compact antenna system for use on extremely compact and tiny spacecraft. Consequently, the very limited geometrical size of required antenna configurations generates several challenges facing proposed metasurface-based antenna design.

The research results of the work we have done thus far offer a noteworthy option for communications between extremely small and ultra-compact spacecraft. The reflection coefficients for both the cross-patch antenna alone and the metasurface sandwich configuration are presented in figure 6. The second one is demonstrated to reduce reflection coefficient (increasing return loss) at a frequency of 8.4 GHz and provide an X-band  $-10$  dB impedance bandwidth of roughly 310 MHz, in spite of the suggested sandwiched metasurface antenna occupying a very tiny size. As a result, the bandwidths obtained are appropriate for use by extremely tiny spacecraft, such as FemtoSats and CubeSats, whose antennas are installed outside of the box. Nevertheless, the cross-patch antenna, lacking a sandwiched metasurface, produces a bi-directional radiation pattern, allowing for the utilization of a significant amount of electromagnetic energy to enhance the peak gain by the sandwiched metasurface. Furthermore, because of the significant level of

back-lobe emission, interactions with spacecraft elements are extremely significant. From this point forward, the suggested sandwiched metasurface improves the suggested antenna design's efficacy for extremely low-cost space missions employing tiny spacecraft. Moreover, figure 7 displays the 2D gain of both the sandwiched metasurface antenna and the cross-patch antenna alone at 8.4 GHz. It shows that, without changing the antenna thickness, sandwiching the suggested metasurface between the cross-patch antenna and the ground plane greatly affects the peak gain, which is the primary characteristic of satellite and spacecraft antennas. As a result, EM interferences are reduced and the back-lobe level is decreased. At the same operating frequency, the peak gain increases from 4.67 dBi to 5.80 dBi, greatly increasing the transmission efficiency and then the whole mission success.

This is due to the fact that when the antenna is set to the sandwiched metasurface's resonance frequency, the emitted electric field is dispersed across an expanded radiating area, increasing the antenna's gain and reducing back-lobe emission. This occurs as a result of the metasurface reflecting back radiation from the antenna outside the spacecraft body after absorbing it. Without altering the physical length

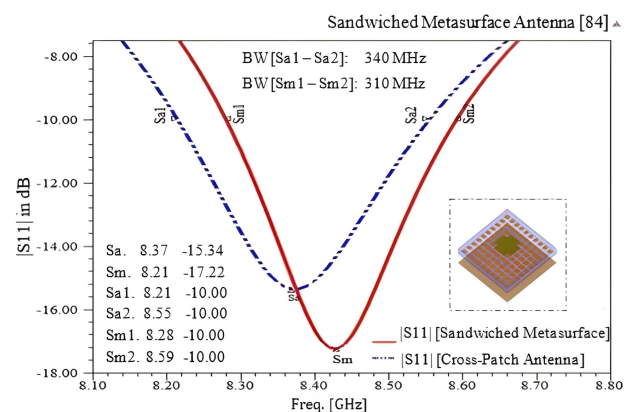
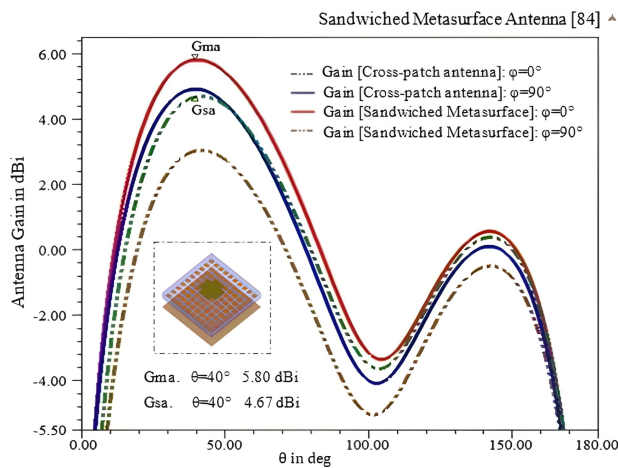


Figure 6. —S11— coefficients of proposed configurations versus frequency [79].



**Figure 7.** 2D gain plots of the cross-patch alone and metasurfaced antenna at 8.4 GHz [79].

and width of the suggested cross-patch antenna, the created sandwiched metasurface is introduced through the employment of  $10 \times 10$  crossing unit cells that are oriented at a  $45^\circ$  angle to increase the peak gain and return loss. Despite its small size of  $29 \times 29 \text{ mm}^2$  at X-band, the proposed sandwiched metasurface antenna achieves a wide bandwidth of approximately 310 MHz and a peak gain of around 6.0 dBi. This means that the sandwiched metasurface enhances the gain and return loss of an exceptionally compact probe-fed cross-patch antenna at X-band. As a result, the suggested metasurface-based antenna is incredibly light, has a very compact profile, and is very low cost. Moreover, its broad beamwidth angle, extreme stiffness and geometrical properties make it very appropriate for low-cost space missions involving ultra-small spacecraft like 0.5U CubeSats, FemtoSats, and ZeptoSats. Furthermore, due to the previously described features, it may also be used as a primary or secondary antenna in tiny spacecraft like the University Mohammed V in Rabat's UM5-Ribat and UM5-EOSAT CubeSats [80, 89]. Therefore, this sandwiched metasurface has great potential and provides an affordable option for these smart space missions when used in the construction of extremely small or ultra-small spacecraft, especially when subsystem components are highly constrained. More effectively, one sandwiched metasurfaced antenna should be mounted on each face of the spacecraft to provide coverage of nearly  $360^\circ$  around the same operational frequency, allowing the proposed spacecraft to communicate with many earth segments and other spacecraft in a CubeSat constellation or satellite network.

As a result, the extensive analysis reported in this work demonstrates that metasurface-based X-band antennas may achieve good gains, radiate unidirectionally, and have physical dimensions suited for a CubeSat structure. This means that they can be used as primary as well as secondary antennas on a CubeSat spacecraft to ensure communication links with earth stations that have the necessary gain and electric energy according to the desired orbit radius. The same results are achieved in different frequency bands, implying that a metasurface-based antenna may be employed for advanced LEO or deep space CubeSat missions if its

gain exceeds 20 dBi at the CubeSat operating frequency. If the gain is medium, it is suitable for LEO CubeSat missions and CubeSat constellations. Otherwise, it can be used to communicate among CubeSats in a swarm. This implies that the two-way analysis described in this article, which is geometrical and mechanical from one side and electrical from the other, reveals all of the benefits and limitations of an antenna design for a certain CubeSat mission. It leads to decisions regarding which CubeSat configuration, whose orbit and duration, which power, size, and frequency band should be targeted based on the overall objectives of a CubeSat mission. Furthermore, all antenna designs, including the metasurface-based one examined in this paper, can use the whole research. From another perspective, NASA's latest space research success, the Parker solar spacecraft, which became the closest man-made object to the star in late 2024 [90, 91], will encourage us all to keep going in the same direction by evaluating the current antenna designs and determining whether they are appropriate for a particular spacecraft. This will result in making the proper choices before putting the necessary modifications into place and then bringing deep space technology to the attention of university students and aspiring researchers.

## 5. Conclusion

The space and CubeSat communities have recently concentrated on developing the AeroCube, a tiny yet capable platform that will serve as the cornerstone for multiple future missions. Antenna systems must meet distant sensing requirements in a small performance package, especially as CubeSats demonstrate potential for advanced applications. The literature discusses several metasurface-based antenna designs for CubeSats based on their electrical and mechanical requirements. This research reviews many metasurface-based antenna designs proposed by scientists and assesses whether or not they are suitable for use with AeroCubes. Antenna approaches that rely on the utilization of metasurfaces achieve the essential antenna performance for a CubeSat mission without increasing the total physical size of final designs, making them geometrically and mechanically acceptable for compact CubeSat configurations like 1U and 1.5U. The most important features of metasurface-based antennas for small- and ultra-small-sized AeroCubes remain their compactness along with the ability to radiate unidirectionally, achieve acceptable bandwidth, and use less power—all of which are constrained on CubeSats. This extensive review also shows that the X-band metasurface-based configurations result in extremely high appropriateness for all CubeSat designs aiming for long-lived CubeSat flights and direct-to-earth station communications. The present study possesses the capacity to substantially demonstrate the usefulness and effectiveness of using metasurface-based antennas on CubeSats, enabling reliable data transmission and reception aimed at all CubeSat frequencies. Moreover, advancements in Fabry-Perot and reflectarray structures might lead to significant enhancements for deep space applications, advanced LEO AeroCube missions, or in-orbit CubeSat stations such as the UM5-Ribat and UM5-EOSAT CubeSats of University Mohammed V in Rabat.



**Nomenclature:** List of symbols and parameters used for preparing the study.

Symbols/parameters	Concept/meaning	Characteristics
LEO	Low Earth Orbit	Earth centered orbit (<2000 km)
QNM	Quasi Newtonian Method	optimization technique
DNG	Double Negative materials	type of metamaterial structures
LHM	Left-Handed materials	left-handed materials
ZIM	Zero-Index materials	type of metamaterial structures
ENZ	Epsilon Near Zero materials	type of metamaterial structures
MNZ	Mu Near Zero materials	type of metamaterial structures
PMC	Perfect Magnetic Conductors	type of metamaterial structures
HIS	High-Impedance Surface materials	type of metamaterial structures
EBG	Electromagnetic BandGap structures	type of metamaterial structures
AMC	Artificial Magnetic Conductors	type of metamaterial structures
PEC	Perfect Electric Conductors	infinite electrical conductivity
oper. fr.	operating frequency [GHz]	antenna parameter
BWs	Bandwidths	effective frequency bands
-10 dB BW	Impedance bandwidth	antenna parameter
3 dB ARBW	Axial Ratio Bandwidth	antenna parameter
3 dBi GBW	3dB Gain bandwidth	antenna parameter
Rad. Pattern	Radiation Pattern	antenna property
U.D.	Unidirectional	low back-lobe radiation
B.D.	Bidirectional	high back-lobe radiation
O.D.	Omnidirectional	360° radiation pattern
Quasi-O.D.	Quasi-Omnidirectional	360° radiation pattern
M.L.	Multi-Lobes Radiation pattern	several high level lobes
Ant. Pol.	Antenna Polarization	antenna parameter
C.P.	Circular Polarization	type of antenna polarization
L.P.	Linear Polarization	type of antenna polarization
V.P.	Vertical Polarization	type of antenna polarization
EMI	electromagnetic Interferences	unwanted noise
$\lambda_0$	free space wavelength	propagation in infinite space of pure material
MTM	Metamaterial	artificially structured material
—S11—	reflection coefficient	analysis of lossless transmission lines
$\epsilon_r$	relative permittivity	intrinsic property of a dielectric
$\tan \delta$	Dielectric loss tangent	quantitatively dissipation of the energy
$G_t$	gain of the transmitting antenna	antenna parameter in dBi
$G_r$	gain of the Receiving antenna	antenna parameter in dBi
$P_t$	transmitted Power	antenna parameter in Watts
$P_r$	received power	antenna parameter in Watts
downlink	CubeSat-to-Earth	satellite telecommunication
uplink	Earth-to-CubeSat	satellite telecommunication

**Authors contributions**

Authors have contributed equally in preparing and writing the manuscript.

**Availability of data and materials**

The data that support the findings of this study are available from the corresponding author upon reasonable request.

**Conflict of interests**

The authors declare that they have no known competing financial interests or personal relationships that could have appeared to influence the work reported in this paper.

## References

- [1] M. El Bakkali. “Planar antennas with parasitic elements and metasurface superstrate structure for 3U CubeSats.”. *PhD Thesis dissertation, Depr. Elect. Eng., Sidi Mohamed Ben Abdellah University (USMBA)*, 2020.
- [2] Nanoacks Deployer. NASA, 2025. URL <https://www.nasa.gov/content/cubesat-deployment>.
- [3] M. Falduto and W. Peeters. “Trade-off approach for launching smallsats.”. *New Space*, 11(2):71–81, 2023. DOI: <https://doi.org/10.1089/space.2022.0003>.
- [4] J. Chin, R. Coelho, J. Foley, A. Johnstone, R. Nugent, D. Pignatelli, S. Pignatelli, N. Powell, J. Puig-Suari, J. Crusan, C. Galica, W. Horne, C. Norton, and A. Robinson. “CubeSat 101: Basic concepts and processes for first-time CubeSat developers.”. *NASA CubeSat Launch Initiative Resources. 1st ed., M. Aldred et. al, Launch Vehicles Used for CubeSat Launch*, 08, 2017.
- [5] O. Popescu. “Power budgets for CubeSat radios to support ground communications and inter-satellite links.”. *IEEE ACCESS*, 5(X):12618–12625, 2017. DOI: <https://doi.org/10.1109/ACCESS.2017.2721948>.
- [6] J. Puig-Suari, C. Turner, and W. Ahlgren. “Development of the standard CubeSat deployer and a CubeSat class picosatellite.”. *2001 IEEE Aerospace Conf. Proceedings, Bi Sky, MT, USA*, pages 1347–1353, 2001. DOI: <https://doi.org/10.1109/AERO.2001.931726>.
- [7] SHERPA Rideshare Mission. “Earth observation portal company.”. *Earth Observation Portal*, 2025. URL <https://directory.eoportal.org/web/eoportal/satellite-missions/s/sherpa>.
- [8] Falcon 9 launch vehicle. “SpaceX Society.”. *SpaceX*, 2025. URL <https://www.spacex.com/falcon9>.
- [9] N. Chahat, E. Decrossas, D. Gonzalez-Ovejero, O. Yurduseven, M. Radway, R. Hodges, P. Estabrook, J. Baker, D. Bell, T. Cwik, and G. Chattopadhyay. “Advanced CubeSat antennas for deep space and Earth science missions: A review.”. *IEEE Ant. & Prop. Magazine*, 61(5):37–46, 2019. DOI: <https://doi.org/10.1109/MAP.2019.2932608>.
- [10] M. El Bakkali, M. E. Bekkali, G. S. Gaba, J. M. Guerrero, L. Kansal, and M. Masud. “Fully integrated high gain S-Band triangular slot antenna for CubeSat communications.”. *Electronics*, 10(2):156, 2021. DOI: <https://doi.org/10.3390/electronics10020156>.
- [11] A.D. Chaudhari, P. Chand, R. Keley, and K.P. Ray. “Design and development of printed antennas for satellite-based AIS applications.”. *2019 TEQIP III Sponsored Intern. Conf. on Microwave Integrated Circuits, Photonics & Wireless Networks (IMICPW)*, pages 341–344, 2019. DOI: <https://doi.org/10.1109/IMICPW.2019.8933263>.
- [12] K. E. Kedze, H. Wang, S. X. Ta, and I. Park. “Wideband low-profile printed dipole antenna incorporated with folded strips and corner-cut parasitic patches above the ground plane.”. *IEEE Access*, 7:15537–15546, 2019. DOI: <https://doi.org/10.1109/ACCESS.2019.2894812>.
- [13] W. C. Liu and T. Y. Tang. “High-gain patch antenna for CubeSat-based automatic dependent surveillance-broadcast application.”. *Microwave and optical technology letters*, 61(1):187–190, 2019. DOI: <https://doi.org/10.1002/mop.31518>.
- [14] A. H. Naqvi and S. Lim. “Microfluidically polarization-switchable metasurfaced antenna.”. *IEEE Antennas and Wireless Propagation Letters*, 17(12):2255–2259, 2018. DOI: <https://doi.org/10.1109/LAWP.2018.2872108>.
- [15] J. Khan, D. A. Sehrai, and S. Ahmad. “Design and performance comparison of metamaterial based antenna for 4G/5G mobile devices.”. *International Journal of Electronics and Communication Engineering*, 12(6):382–387, 2018.
- [16] N. Hussain, U. Azimov, J. W. Park, S. Y. Rhee, and N. Kim. “A microstrip patch antenna sandwiched between a ground plane and a metasurface for WiMAX applications.”. *2018 Asia-Pacific Microwave Conference (APMC)*, pages 1016–1018, 2018. DOI: <https://doi.org/10.23919/APMC.2018.8617342>.
- [17] R. K. Prajapati and S. S. Lodhi. “Improvement in Parameters of Patch Antenna by Using “Spiral Shapes” Metamaterial Structure.”. *Int. J. Adv. Innovations, Thoughts Ideas*, 2(2):1–5, 2013.
- [18] J. L. D. S. Paiva, J. P. da Silva, A. L. P. D. S. Campos, and H. Dionísio de Andrade. “Using metasurface structures as signal polarisers in microstrip antennas.”. *IET microwaves, antennas & propagation*, 13(1):23–27, 2018. DOI: <https://doi.org/10.1049/iet-map.2018.5112>.
- [19] R. Rajkumar and K. Usha Kiran. “Gain enhancement of compact multiband antenna with metamaterial superstrate.”. *Optical And Microwave Technologies. Lecture Notes in Electrical Engineering, Springer, Singapore*, 468:91–98, 2018. DOI: [https://doi.org/10.1007/978-981-10-7293-2\\_10](https://doi.org/10.1007/978-981-10-7293-2_10).
- [20] M. Elhabchi, M. N. Srifi, and R. Touahni. “A fractal metamaterial antenna for bluetooth, WLAN, WiMAX and X-band Applications.”. *2020 International Conf. on Intelligent Syst. and Comp. Vision (ISCV)*, pages 1–5, 2020. DOI: <https://doi.org/10.1109/ISCV49265.2020.9204208>.
- [21] S. Huang, C. F. Zhou, J. X. Sun, S. S. Yuan, H. Li, X. M. Ding, and X. B. Tang. “A wideband L-probe fed conformal antenna array using metasurface.”. *IEEE Open Journal of Antennas and Propagation*, 2:1175–1183, 2021. DOI: <https://doi.org/10.1109/OJAP.2021.3131242>.
- [22] S. Tretyakov, A. Urbas, and N. Zheludev. “Special issue on the history of metamaterials.”. *J. Opt.*, 19:080404, 2017.
- [23] S. X. Ta and I. Park. “Metasurface-based circularly polarized patch array antenna using sequential phase feed.”. *2017 International Workshop on Antenna Technology: Small Antennas, Innovative Structures, and Applications (iWAT)*, pages 24–25, 2017. DOI: <https://doi.org/10.1109/IWAT.2017.7915287>.
- [24] X. Qing and Z. N. Chen. “Broadband circularly polarized antenna using metasurface.”. *2017 Progress in Electromagnetics Research Symposium-Fall (PIERS-FALL)*, pages 2940–2944, 2017. DOI: <https://doi.org/10.1109/PIERS-FALL.2017.8293636>.
- [25] H. Zhu, W. S. W. Cheung, and T. I. Yuk. “Antenna reconfiguration using metasurfaces.”. *2014 Progress in Electromagnetics Research Symposium (PIERS 2014)*, pages 2400–2404, 2014.
- [26] Y. Huang, J. Li, and G. Wen. “Wideband low-profile circular polarization slot antenna based on metasurface.”. *2017 IEEE International Symposium on Antennas and Propagation & USNC/URSI National Radio Science Meeting*, pages 471–472, 2017. DOI: <https://doi.org/10.1109/APUSNCURSINRSM.2017.8072278>.

- [27] Y. Jia, Y. Liu, S. Gong, W. Zhang, and G. Liao. "A low-RCS and high-gain circularly polarized antenna with a low profile." *IEEE Antennas and Wireless Propagation Letters*, 16:2477–2480, 2017. DOI: <https://doi.org/10.1109/LAWP.2017.2725380>.
- [28] H. L. Zhu, S. W. Cheung, and T. I. Yuk. "Miniaturization of patch antenna using metasurface." *Microwave and optical technology letters*, 57(9):2050–2056, 2015. DOI: <https://doi.org/10.1002/mop.29275>.
- [29] Z. Wu, L. Li, Y. Li, and X. Chen. "Metasurface superstrate antenna with wideband circular polarization for satellite communication application." *IEEE antennas and wireless propagation letters*, 15:374–377, 2016. DOI: <https://doi.org/10.1109/LAWP.2015.2446505>.
- [30] Z. Wu, H. Liu, and L. Li. "Polarization reconfigurable metasurface superstrate antenna with low profile." *2016 10th European Conference on Antennas and Propagation (EuCAP)*, pages 1–2, 2016. DOI: <https://doi.org/10.1109/EuCAP.2016.7481413>.
- [31] J. Wang, H. Wong, Z. Ji, and Y. Wu. "Broadband CPW-fed aperture coupled metasurface antenna." *IEEE Antennas and Wireless Propagation Letters*, 18(3):517–520, 2019. DOI: <https://doi.org/10.1109/LAWP.2019.2895618>.
- [32] S. X. Ta and I. Park. "Compact wideband circularly polarized patch antenna array using metasurface." *IEEE Antennas and Wireless Propagation Letters*, 16:1932–1936, 2017. DOI: <https://doi.org/10.1109/LAWP.2017.2689161>.
- [33] N. Nasimuddin, Z. N. Chen, and X. Qing. "Bandwidth enhancement of a single-feed circularly polarized antenna using a metasurface: Metamaterial-based wideband CP rectangular microstrip antenna." *IEEE Antennas and Propagation Magazine*, 58(2):39–46, 2016. DOI: <https://doi.org/10.1109/MAP.2016.2520257>.
- [34] H. L. Zhu, X. H. Liu, S. W. Cheung, and T. I. Yuk. "Frequency-reconfigurable antenna using metasurface." *IEEE Transactions on Antennas and Propagation*, 62(1):80–85, 2014. DOI: <https://doi.org/10.1109/TAP.2013.2288112>.
- [35] R. Xi, L. Li, T. Zhang, and P. Wang. "Dissimilar metasurface superstrate high directivity antenna." *2017 6th Asia-Pacific Conference on Antennas and Propagation (APCAP)*, pages 1–3, 2017. DOI: <https://doi.org/10.1109/APCAP.2017.8420455>.
- [36] J. Huang, W. Lin, and Y. J. Guo. "A ultra-light high gain circularly-polarized antenna array for mobile satellite terminals." *2018 IEEE International Symposium on Antennas and Propagation & USNC/URSI National Radio Science Meeting*, pages 1233–1234, 2018. DOI: <https://doi.org/10.1109/APUSNCURSINRSM.2018.8609369>.
- [37] C. Xue, Q. Lou, and Z. N. Chen. "Broadband double-layered Huygens' metasurface lens antenna for 5G millimeter-wave systems." *IEEE Transactions on Antennas and Propagation*, 68(3):1468–1476, 2020. DOI: <https://doi.org/10.1109/TAP.2019.2943440>.
- [38] T. Li and Z. N. Chen. "Design of dual-band metasurface antenna." *2018 International Workshop on Antenna Technology (iWAT)*, pages 1–3, 2018. DOI: <https://doi.org/10.1109/IWAT.2018.8379213>.
- [39] O. Yurduseven, C. Lee, N. Chahat, D. Gonzalez-Ovejero, M. Etorre, R. Sauleau, and G. Chattopadhyay. "Design of a quasi-optical Si/GaAs W-band beam-forming metasurface antenna." *2019 IEEE International Symposium on Antennas and Propagation and USNC-URSI Radio Science Meeting*, pages 1713–1714, 2019. DOI: <https://doi.org/10.1109/APUSNCURSINRSM.2019.8888637>.
- [40] N. Hussain and I. Park. "Performance of multiple-feed metasurface antennas with different numbers of patch cells and different substrate thicknesses." *Appl. Computational Electromagnetics Society Journal*, 33(03):298–304, 2021.
- [41] N. Hussain and I. Park. "High gain metasurface antenna with multiple feeding structure." *11th International Cong. on Engineered Materials Platforms for Novel Wave Phenomena (Metamaterials)*, pages 253–255, 2017. DOI: <https://doi.org/10.1109/MetaMaterials.2017.8107909>.
- [42] W. Ji, J. Chang, H. X. Xu, J. R. Gao, S. Gröblacher, H. P. Urbach, and A. J. Adam. "Recent advances in metasurface design and quantum optics applications with machine learning, physics-informed neural networks, and topology optimization methods." *Light: Science & Applications*, 12(1):169, 2023. DOI: <https://doi.org/10.1038/s41377-023-01218-y>.
- [43] H. T. Chen, A. J. Taylor, and N. Yu. "A review of metasurfaces: Physics and applications." *Reports on progress in physics*, 79(7):076401, 2016. DOI: <https://doi.org/10.1088/0034-4885/79/7/076401>.
- [44] S. S. Bukhari, J. Vardaxoglou, and W. Whittow. "A metasurfaces review: Definitions and applications." *Applied Sciences*, 9(13):2727, 2019. DOI: <https://doi.org/10.3390/app9132727>.
- [45] J. Hu, S. Bandyopadhyay, Y. H. Liu, and L. Y. Shao. "A review on metasurface: From principle to smart metadevices." *Frontiers in Physics*, 8:586087, 2021. DOI: <https://doi.org/10.3389/fphy.2020.586087>.
- [46] X. Zhao, Z. Sun, L. Zhang, Z. Wang, R. Xie, J. Zhao, R. You, and Z. You. "Review on metasurfaces: An alternative approach to advanced devices and instruments." *Advanced Devices & Instrumentation*, pages 1–19, 2022. DOI: <https://doi.org/10.34133/2022/9765089>.
- [47] H. Jeong, H. Kim, and S. Lee. "Review of metasurfaces with extraordinary flat optic functionalities." *Curr. Opt. Photon*, 8(1):16–29, 2024. DOI: <https://doi.org/http://dx.doi.org/10.3807/COPP.2024.8.1.16>.
- [48] W. L. Hsu, Y. C. Chen, S. P. Yeh, Q. C. Zeng, Y. W. Huang, and C. M. Wang. "Review of metasurfaces and metadevices: Advantages of different materials and fabrications." *Nanomaterials*, 12(12):1973, 2022. DOI: <https://doi.org/10.3390/nano12121973>.
- [49] H. Malekpoor. "Broadband printed tapered slot antenna fed by CPW fulfilled with planar artificial magnetic conductor for X-band operation." *Advanced Electromagnetics*, 12(1):1–10, 2023. DOI: <https://doi.org/10.7716/aem.v12i1.2087>.
- [50] H. Malekpoor and M. Hamidkhani. "Analysis of high gain wide-band 2×2 printed slot array with AMC surface by presenting equivalent transmission line model for C and X-Band applications." *IEEE Access*, 11:59164–59173, 2023. DOI: <https://doi.org/10.1109/ACCESS.2023.3285774>.
- [51] B. Bandyopadhyay, S. Bhattacharya, R. K. Jaiswal, M. Saikia, and K. V. Srivastava. "Wideband RCS reduction of a linear patch antenna array using AMC metasurface for stealth applications." *IEEE Access*, 11:127458–127467, 2023. DOI: <https://doi.org/10.1109/ACCESS.2023.3332120>.
- [52] B. T. P. Madhav, J. Vani, R. R. Priyanka, B. P. Nadh, and M. C. Rao. "Concentric ring loaded monopole antenna with AMC backed for Wearable applications." *Journal of Physics: Conference Series*, 1804(1):012191, 2021. DOI: <https://doi.org/10.1088/1742-6596/1804/1/012191>.
- [53] S. K. Patel, C. D. Bui, T. K. Nguyen, J. Parmar, and Q. M. Ngo. "Numerical investigation of frequency reconfigurable antenna with liquid metamaterials for X-band." *Journal of Advanced Engineering and Computation*, 6(1):60–72, 2022. DOI: <https://doi.org/http://dx.doi.org/10.55579/jaec.202261.362>.
- [54] J. Undrakonda and R. K. Upadhyayula. "Isolation analysis of miniaturized metamaterial-based MIMO antenna for X-band radar applications using machine learning model." *Prog. Electromagn. Res. C*, 124:135–153, 2022. DOI: <https://doi.org/http://dx.doi.org/10.2528/PIERC22080203>.

- [55] O. Borazjani, M. Naser-Moghadasi, J. Rashed-Mohassel, and R. A. Sadeghzadeh. "Bandwidth improvement of planar antennas using a single-layer metamaterial substrate for X-band application.". *International Journal of Microwave and Wireless Technologies*, 12 (9):906–914, 2020.  
DOI: <https://doi.org/10.1017/S1759078720000264>.
- [56] C. X. Bai, Y. J. Cheng, Y. R. Ding, and J. F. Zhang. "A metamaterial-based S/X-Band shared-aperture phased-array antenna with wide beam scanning coverage.". *IEEE Transactions on Antennas and Propagation*, 68(6):4283–4292, 2020.  
DOI: <https://doi.org/10.1109/TAP.2020.2970096>.
- [57] O. Borazjani, M. Naser-Moghadasi, J. Rashed-Mohassel, and R. Sadeghzadeh. "Design and fabrication of a new high gain multilayer negative refractive index metamaterial antenna for X-band applications.". *International Journal of RF and Microwave Computer-Aided Engineering*, 30(9):e22284, 2020.  
DOI: <https://doi.org/10.1002/mmce.22284>.
- [58] M. Gaharwar and D. C. Dhukarya. "X-band multilayer stacked microstrip antenna using novel electromagnetic band-gap structures.". *IETE Journal of Research*, 69(4):2015–2024, 2021.  
DOI: <https://doi.org/10.1080/03772063.2021.1883484>.
- [59] J. Jiang, Y. Li, L. Zhao, and X. Liu. "Wideband MIMO directional antenna array with a simple meta-material decoupling structure for X-band applications.". *Applied Computational Electromagnetics Society Journal (ACES)*, 35(5):556–566, 2020.
- [60] A. Majeed, J. Zhang, and H. A. Khan. "Metasurface-based circularly polarized slot antenna for X-band applications.". *Research Square*, 2024.  
DOI: <https://doi.org/10.21203/rs.3.rs-4208189/v1>.
- [61] S. Charola, S. K. Patel, J. Parmar, and R. Jadeja. "Multiband Jerusalem cross-shaped angle insensitive metasurface absorber for X-band application.". *Journal of Electromagnetic Waves and Applications*, 36(2):180–192, 2021.  
DOI: <https://doi.org/10.1080/09205071.2021.1960643>.
- [62] D. Samantaray and S. Bhattacharyya. "A gain-enhanced slotted patch antenna using metasurface as superstrate configuration.". *IEEE Transactions on Antennas and Propagation*, 68(9):6548–6556, 2020.  
DOI: <https://doi.org/10.1109/TAP.2020.2990280>.
- [63] R. Swain, D. K. Naik, and A. K. Panda. "Low-loss ultra-wideband beam switching metasurface antenna in X-band.". *IET Microwaves, Antennas & Propagation*, 14(11):1216–1221, 2020.  
DOI: <https://doi.org/10.1049/iet-map.2019.0994>.
- [64] M. Guo, W. Wang, and P. Huang. "Double-layer metasurface-based low profile broadband X-band microstrip antenna.". *IET Microwaves, Antennas & Propagation*, 14(9):919–927, 2020.  
DOI: <https://doi.org/10.1049/iet-map.2019.1098>.
- [65] S. Genovesi and F. A. Dicandia. "Characteristic modes analysis of a near-field polarization-conversion metasurface for the design of a wideband circularly polarized X-band antenna.". *IEEE Access*, 10:88932–88940, 2022.  
DOI: <https://doi.org/10.1109/ACCESS.2022.3200303>.
- [66] L. Teodorani, F. Vernì, G. Giordanengo, R. Gaffoglio, and G. Vecchi. "Experimental demonstration of beam scanning of dual-metasurface antenna.". *Electronics*, 12(8):1833, 2023.  
DOI: <https://doi.org/10.3390/electronics12081833>.
- [67] X. Ren, Y. Bao, Z. Wu, Q. W. Lin, and H. Wong. "A low-profile wideband metasurface antenna with fan-beam radiation.". *IEEE Open Journal of Antennas and Propagation*, 3:745–751, 2022.  
DOI: <https://doi.org/10.1109/OJAP.2022.3187378>.
- [68] J. Wang, W. Wang, A. Liu, M. Guo, and Z. Wei. "Miniaturized dual-polarized metasurface antenna with high isolation.". *IEEE Antennas and Wireless Propagation Letters*, 20(3):337–341, 2021.  
DOI: <https://doi.org/10.1109/LAWP.2021.3049856>.
- [69] T. Wu, J. L. Li, S. Zhang, and J. Chen. "Design of broadband circularly polarized metasurface antenna array with gain enhancement.". *International Journal of RF and Microwave Computer-Aided Engineering*, 30(12):e22446, 2020.  
DOI: <https://doi.org/10.1002/mmce.22446>.
- [70] L. Leszkowska, M. Rzymowski, K. Nyka, and L. Kulas. "High-gain compact circularly polarized X-band superstrate antenna for CubeSat applications.". *IEEE Antennas and Wireless Propagation Letters*, 20(11):2090–2094, 2021.  
DOI: <https://doi.org/10.1109/LAWP.2021.3076673>.
- [71] H. Wang, X. F. Dong, J. Shen, S. L. Zhou, H. F. Wang, and Z. B. Wang. "Fan-beam antenna design based on metasurface lenses.". *International Journal of RF and Microwave Computer-Aided Engineering*, 31(4):e22582, 2021.  
DOI: <https://doi.org/10.1002/mmce.22582>.
- [72] S. Dey and S. Dey. "Ultrathin single layer transmissive dual-band linear to circular converter for non-adjacent dual orthogonal circularly polarized antenna.". *IEEE Access*, 12:65981–65996, 2024.  
DOI: <https://doi.org/10.1109/ACCESS.2024.3398144>.
- [73] Z. Yang, T. Wu, S. Zhang, Z. Liu, D. Yang, and W. Cao. "A broadband wide-angle linear-to-circular polarization converter based on stripline metasurface.". *IEEE Access*, 9:163204–163213, 2021.  
DOI: <https://doi.org/10.1109/ACCESS.2021.3134064>.
- [74] B. Feng, J. Lai, Q. Zeng, and K. L. Chung. "A dual-wideband and high gain magneto-electric dipole antenna and its 3D MIMO system with metasurface for 5G/WiMAX/WLAN/X-band applications.". *IEEE Access*, 6:33387–33398, 2018.  
DOI: <https://doi.org/10.1109/ACCESS.2018.2848476>.
- [75] B. Li, X. Liu, H. Shi, C. Yang, Q. Chen, and A. Zhang. "Planar phase gradient metasurface antenna with low RCS.". *IEEE Access*, 6:78839–78845, 2018.  
DOI: <https://doi.org/10.1109/ACCESS.2018.2885356>.
- [76] Q. Chen and H. Zhang. "High-gain circularly polarized Fabry-Pérot patch array antenna with wideband low-radar-cross-section property.". *IEEE Access*, 7:8885–8889, 2019.  
DOI: <https://doi.org/10.1109/ACCESS.2018.2890691>.
- [77] P. Zhang, L. Li, X. Zhang, H. Liu, and Y. Shi. "Design, measurement and analysis of near-field focusing reflective metasurface for dual-polarization and multi-focus wireless power transfer.". *IEEE access*, 7:110387–110399, 2019.  
DOI: <https://doi.org/10.1109/ACCESS.2019.2934135>.
- [78] Y. Fan, J. Wang, Y. Li, J. Zhang, Y. Han, and S. Qu. "Low-RCS and high-gain circularly polarized metasurface antenna.". *IEEE Transactions on Antennas and Propagation*, 67(12):7197–7203, 2019.  
DOI: <https://doi.org/10.1109/TAP.2019.2920355>.
- [79] B. Benhmimou, N. Hussain, N. Gupta, R. A. Laamara, S. K. Arora, J. M. Guerrero, and M. El Bakkali. "Sandwiched metasurface antenna for small spacecrafts in IoT infrastructure.". *Internet of Things*, pages 117–127, 2023.  
DOI: [https://doi.org/10.1007/978-3-031-33808-3\\_7](https://doi.org/10.1007/978-3-031-33808-3_7).
- [80] B. Benhmimou, F. Omari, N. Gupta, K. El Khadiri, R. Ahl Laamara, and M. El Bakkali. "Air-gap reduction and antenna positioning of an X-band bow tie slot antenna on 2U CubeSats.". *Journal of Applied Engineering and Technological Science (JAETS)*, 6(1): 86–102, 2024.  
DOI: <https://doi.org/10.37385/jaets.v6i1.6158>.
- [81] E. Dotto and A. Zinzi. "Impact observations of asteroid dimorphos via Light Italian CubeSat for imaging of asteroids (LICIAcube)". *Nat Commun*, 14(3055), 2023.  
DOI: <https://doi.org/10.1038/s41467-023-38705-0>.
- [82] E.L. Shkolnik. "On the verge of an astronomy CubeSat revolution.". *Nat. Astron.*, 2:374–378, 2018.  
DOI: <https://doi.org/10.1038/s41550-018-0438-8>.



- [83] J.D. Liddle, A.P. Holt, S.J. Jason, K. A. Donnell, and E. J. Stevens. “Space science with CubeSats and nanosatellites.”. *Nat Astron*, 4: 1026–1030, 2020. DOI: <https://doi.org/10.1038/s41550-020-01247-2>.
- [84] E. Gibney. “CubeSats set for deep space: If they can hitch a ride.”. *Nature*, 535:19–20, 2016. DOI: <https://doi.org/10.1038/535019a>.
- [85] Y. Kajimura, N. Hirota, K. Nakata, Y. Oshio, and I. Funaki. “Development and operation demonstration of pulsed plasma thruster for 2U-CubeSat.”. *Journal of Evolving Space Activities*, 2 (143), 2024. DOI: <https://doi.org/10.57350/jesa.143>.
- [86] K. Taguchi, K. Tanimoto, T. Omoto, T. Watanabe, K. Kuwata, K. Nagamine, Y. Sato, H. Seki, and T. Suzuki. “Development of CubeSat ”WE WISH” deployed from ISS.”. *Intern. Journal of Microgravity Science and Application*, 30(3):143, 2013. DOI: <https://doi.org/10.15011/jasma.30.3.143>.
- [87] J. Nakaya, H. Tsuchiya, T. Sakamoto, T. Kato, Y. Kajimura, K. Kitamura, S. Ueta, and T. Takada. “Development and application of a 2U CubeSat ground Model for space technology education.”. *Journal of JSEE*, 68(2):2\_60 – 2\_65, 2020. DOI: <https://doi.org/10.4307/jsee.68.2.60>.
- [88] N. Uezono, Y. Sasaoka, J. Nakaya, H. Tsuchiya, Y. Kajimura, K. Kitamura, S. Ueta, and T. Takada. “Development and application of a CubeSat ground Model for space technology education.”. *Journal of JSEE*, 67(2):2\_95 – 2\_100, 2019. DOI: <https://doi.org/10.4307/jsee.67.2.95>.
- [89] UM5-Ribat and UM5-EOSat CubeSats. *Space Watch Africa*, 2025. URL <https://spacewatchafrica.com/mohammed-v-university-and-spacex-launch-two-nanosatellites/>.
- [90] NASA’s Parker Solar Probe Makes History with Closest Pass to Sun. *NASA’s Website*, 2025. URL [NASA’s Website](https://www.nasa.gov/parker-solar-probe).
- [91] Parker Solar Probe. *Website of Johns Hopkins Applied Physics Laboratory*, 2025. URL <https://www.jhuapl.edu/destinations/missions/parker-solar-probe>.